THE JOURNAL OF BIOLOGICAL CHEMISTRY
Vol. 277, No. 37, Issue of September 13, pp. 34424–34433, 2002

Printed in U.S.A.

Mitochondrial Alterations Induced by the p13^{II} Protein of Human T-cell Leukemia Virus Type 1

CRITICAL ROLE OF ARGININE RESIDUES*

Received for publication, March 28, 2002, and in revised form, June 13, 2002
Published, JBC Papers in Press, July 1, 2002, DOI 10.1074/jbc.M203023200

Donna M. D'Agostino‡§, Laura Ranzato¶, Giorgio Arrigoni‖, Ilaria Cavallari‡, Francesca Belleudi, Maria Rosaria Torrisi**, Micol Silic-Benussi‡, Tiziana Ferro‡, Valeria Petronilli¶, Oriano Marin‖, Luigi Chieco-Bianchi‡, Paolo Bernardi¶, and Vincenzo Ciminale‡ ‡‡**

*From the ‡Department of Oncology and Surgical Sciences, University of Padova, Padova 35128, Italy, Consiglio Nazionale delle Ricerche Institute of Neuroscience at the Departments of ¶Biomedical Sciences and ‖Biological Chemistry, University of Padova, Padova 35121, Italy, and the **Department of Experimental Medicine and Pathology, University of Rome La Sapienza, Rome, 00161 Italy*

Human T-cell leukemia virus type 1 encodes a number of "accessory" proteins of unclear function; one of these proteins, p13^{II}, is targeted to mitochondria and disrupts mitochondrial morphology. The present study was undertaken to unravel the function of p13^{II} through (i) determination of its submitochondrial localization and sequences required to alter mitochondrial morphology and (ii) an assessment of the biophysical and biological properties of synthetic peptides spanning residues 9–41 (p13$^{9-41}$), which include the amphipathic mitochondrial-targeting sequence of the protein. p13$^{9-41}$ folded into an α helix in micellar environments. Fractionation and immunogold labeling indicated that full-length p13^{II} accumulates in the inner mitochondrial membrane. p13$^{9-41}$ induced energy-dependent swelling of isolated mitochondria by increasing inner membrane permeability to small cations (Na^+, K^+) and released Ca^{2+} from Ca^{2+}-preloaded mitochondria. These effects as well as the ability of full-length p13^{II} to alter mitochondrial morphology in cells required the presence of four arginines, forming the charged face of the targeting signal. The mitochondrial effects of p13$^{9-41}$ were insensitive to cyclosporin A, suggesting that full-length p13^{II} might alter mitochondrial permeability through a permeability transition pore-independent mechanism, thus distinguishing it from the mitochondrial proteins Vpr and X of human immunodeficiency virus type 1 and hepatitis B virus, respectively.

HTLV-1[1] is a complex retrovirus that is associated with two distinct pathologies, a leukemia/lymphoma of mature $CD4^+$ T-cells and a neurodegenerative disease (tropical spastic paraparesis/HTLV-associated myelopathy). Adult T-cell leukemia/lymphoma and tropical spastic paraparesis/HTLV-associated myelopathy arise in a minority (2–5%) of HTLV-1-infected subjects after a latency period of years to decades. Although HTLV-1 was the first retrovirus demonstrated to cause neoplasia in humans, a number of aspects of its life cycle and pathogenic properties are still poorly understood (for recent reviews of HTLV-1, see Refs. 1 and 2). The viral transcriptional regulator Tax is known to play a critical role in HTLV-1-associated cell immortalization through its ability to deregulate the expression of a vast array of cellular genes and interfere with cell cycle checkpoints. Although it is well established that HTLV-1 is oncogenic *in vitro*, neoplastic transformation of primary human lymphocytes cannot be attained by transducing Tax alone, suggesting that other viral (and host) determinants are also required for the emergence of adult T-cell leukemia/lymphoma. Furthermore, the low prevalence and long latency of leukemia in HTLV-1-infected individuals suggest the existence of mechanisms holding the oncogenic potential of the virus at bay, resulting in efficient adaptation to the host. Even less is known regarding the pathogenesis of tropical spastic paraparesis/HTLV-associated myelopathy, although a cytotoxic T-lymphocyte-mediated autoimmune mechanism has been postulated.

To gain further insight into the mechanisms governing HTLV-1 replication and pathogenesis, a number of studies are currently focusing on recently described "accessory" proteins encoded in ORFs x-I and x-II, which are located in a 3′ portion of the viral genome termed the X region (3–5). Although the accessory ORFs are dispensable for virus propagation and immortalization of T-cells *in vitro* (6–8), they are essential for efficient viral propagation in animal models (9–11). In addition, cell-mediated immune responses against these gene products have been demonstrated in infected individuals (12), thus providing strong evidence that these proteins are expressed during the natural history of HTLV-1 infection.

We demonstrated that one of the gene products of the x-II ORF, named p13^{II}, is selectively targeted to mitochondria. Expression of p13^{II} results in specific alterations in mitochondrial morphology and distribution from an extensively intercon-

* This work was supported in part by Grants from the Istituto Superiore di Sanita (ISS AIDS research program 9204-28) and grants from Associazione Italiana per la Ricerca sul Cancro (to L. C.-B. and P. B.), the Fondazione Italiana per la Ricerca sul Cancro, and the Ministero per l'Università e la Ricerca Scientifica e Tecnologica. The laboratory at the Department of Oncology and Surgical Sciences participated in the concerted action HTLV European Research Network of the European Commission Biomed Program. The costs of publication of this article were defrayed in part by the payment of page charges. This article must therefore be hereby marked "*advertisement*" in accordance with 18 U.S.C. Section 1734 solely to indicate this fact.

§ Recipient of a fellowship from Fondazione Italiana per la Ricerca sul Cancro.

‡‡ To whom correspondence should be addressed: Dipartimento di Scienze Oncologiche e Chirurgiche, Università di Padova, via Gattamelata 64, 35128 Padova, Italy. Tel.: 39-049-821-5885; Fax: 39-049-807-2854; E-mail: v.ciminale@unipd.it.

[1] The abbreviations used are: HTLV-1, human T-cell leukemia virus type 1; CD, circular dichroism; Cox, cytochrome oxidase; CsA, cyclosporin A; $\Delta\psi$, mitochondrial inner membrane potential; DNP, dinitrophenol; MOPS, 4-morpholinepropanesulfonic acid; MTS, mitochondrial-targeting sequence; ORF, open reading frame; p13$^{9-41}$, synthetic peptide spanning residues 9–41 of p13^{II}; PTP, permeability transition pore; PBS, phosphate-buffered saline.

nected network of string-like structures to clusters of spheroid bodies, suggesting that p13^{II} might interfere with mitochondrial function *in situ* (13). This observation along with the findings that the p13^{II}-coding sequence is conserved among HTLV-1 isolates, that its mRNA is expressed during HTLV-1 infection and disease (5, 14), and that cytotoxic T-lymphocytes against the x-II ORF are detected in HTLV-1-infected individuals (12) indicate that the protein might exert a significant biological role in viral replication and/or pathogenesis. The present study was undertaken to unravel the function of p13^{II} through (i) determination of its submitochondrial localization and sequences required to induce the alterations in mitochondrial morphology and (ii) an assessment of the biophysical and biological properties of a set of synthetic peptides spanning residues 9–41, which include the amphipathic MTS of the protein. Results demonstrated the functional importance of a cluster of MTS arginines and indicated that the protein accumulates in the inner mitochondrial membrane. On the basis of observations made with the synthetic peptides, we propose that p13^{II} increases mitochondrial permeability to small cations (*e.g.* Ca^{2+}, Na^{+}, and K^{+}), causing swelling of the organelle and depolarization.

MATERIALS AND METHODS

Peptide Synthesis—Peptides were synthesized by solid phase methods and 9-fluorenilmethoxycarbonyl chemistry (15) using an Applied Biosystems (Foster City, CA) model 431 A peptide synthesizer (improved in our laboratories as described in Marin *et al.* (16). After cleavage with trifluoroacetic acid, the peptides were purified to homogeneity by reverse phase-high performance liquid chromatography on a Waters (Milford, MA) prepNova-Pak HR C18 column with a linear gradient of 10–45% acetonitrile at a flow rate of 12 ml/min. Peptide molecular weights were confirmed by mass spectroscopy using a matrix-assisted laser desorption ionization time-of-flight spectrometer (Maldi-1; Kratos-Shimadzu, Manchester, England).

Circular Dichroism—CD spectra were recorded with a Jasco (Easton, MD) J-170 spectropolarimeter. The instrument was calibrated with *d*-(+)-10-camphorsulfonic acid. Far-UV CD spectra were recorded at 25 °C at a peptide concentration of 15 μM in buffers specified in the legend to Fig. 2 using 0.1-cm path length quartz cells. The mean residue ellipticity [Θ] (deg·cm^2·dmol^{-1}) was calculated from the formula $[\Theta]_{MRW} = (\Theta_{obs}/10)MRW/lc$), where Θ_{obs} is the observed ellipticity at a given wavelength, MRW is the mean residue weight of the peptide(s), l is the cuvette path length in cm, and c is the peptide concentration in g/ml. Lipid vesicles were prepared from dioleoylphosphatidylglycerol in trichloromethane. After evaporating the organic solvent under an argon stream, the dried lipid was dissolved in Tris/HCl buffer to obtain a final lipid concentration of 1.7 mM and sonicated for about 15 min until the solution became transparent.

Plasmids and Transfections—The p13^{II} ORF was obtained from HTLV-1 molecular clone pCS-HTLV-1 (17) and cloned into vector pSG5 (Stratagene, La Jolla, CA), resulting in plasmid pSGp13^{II}. Mutations in the p13^{II} ORF were introduced by site-directed mutagenesis (QuikChange kit, Stratagene) and verified by cycle sequencing (fmol kit, Promega, Madison, WI). PCR amplifications were carried out using Vent DNA polymerase (New England Biolabs, Beverly, MA) in a GeneAmp 9600 thermal cycler (PerkinElmer Life Sciences). Restriction enzymes were purchased from New England Biolabs and Roche Molecular Biochemicals, and synthetic oligonucleotides were purchased from Invitrogen. Plasmids were purified by chromatography (Jetstar kit, Genomed, Bad Oeynhausen, Germany) and transfected into HeLa cells or the HeLa-derived cell line Hltat (Ref. 18; used due to their high transfection efficiency) by calcium phosphate coprecipitation.

Mitochondrial Fractionation—Crude preparations of mitochondria were obtained from Hltat cells as follows. One day after transfection with pSGp13^{II}, cells were scraped into PBS, pelleted, and then resuspended in a mitochondrial isolation buffer consisting of 300 mM sucrose, 10 mM MOPS, pH 7.4, 1 mM EDTA, and 4 mM KH_2PO_4 (19) with 200 μM phenylmethylsulfonyl fluoride and 10 μg/ml leupeptin added as protease inhibitors. The suspension was passed 10 times through a 26-gauge needle and centrifuged 2 times at 625 × *g* for 10 min in a swinging bucket rotor to remove intact cells and large debris. The clarified supernatant was centrifuged at 17,500 × *g* for 15 min; the resulting pellets containing mitochondria were resuspended in mitochondrial isolation buffer and recentrifuged. For Triton X-114 fractionation assays, mitochondrial pellets were resuspended in 10 mM Tris, pH 7.5, 150 mM NaCl, 200 μM phenylmethylsulfonyl fluoride, 10 μg/ml leupeptin, and 1% Triton X-114 and processed as described by Bordier (20) with the exception that all volumes were reduced by one-half; supernatants and pellets were solubilized and analyzed by SDS-PAGE/immunoblotting. Sodium carbonate extraction (21) was performed as follows. Washed mitochondrial pellets were resuspended in 100 mM sodium carbonate, pH 11.5, and incubated on ice for 30 min. The alkaline mixture was then combined with enough 2.5 M sucrose prepared in 100 mM sodium carbonate to yield a final sucrose concentration of 1.6 M. This suspension was placed in an ultracentrifuge tube and overlaid with 1.25 M sucrose, 100 mM sodium carbonate followed by a layer of 250 mM sucrose, 100 mM sodium carbonate and centrifuged at 47,000 rpm for 2 h in an SW60.1 rotor (Beckman Instruments). The step gradient was collected in 2 fractions, the 0.25–1.25 M sucrose interface plus the 1.25 M sucrose layer, containing membrane-integrated proteins, and the 1.6 M sucrose layer, containing proteins not inserted into membranes. The fractions were diluted with water to reduce the sucrose concentration to 500 mM, and proteins were precipitated with 12% trichloroacetic acid, solubilized, and separated by SDS-PAGE/immunoblotting. Digitonin fractionation assays were performed by resuspending mitochondria in a sucrose-based solution (250 mM sucrose, 10 mM HEPES, pH 7.1, 10 mM KCl, 1.5 mM $MgCl_2$, 1 mM EDTA, 1 mM EGTA, 200 μM phenylmethylsulfonyl fluoride, and 10 μg/ml leupeptin) with or without 0.5% digitonin; after incubation for 1 min on ice the suspensions were centrifuged at 17,500 × *g* for 15 min, and resulting supernatants and pellets were solubilized and analyzed by SDS-PAGE/immunoblotting.

SDS-PAGE/Immunoblotting—Solubilized proteins were separated in SDS-polyacrylamide gels (15% total; 37.5:1 acrylamide:bisacrylamide) along with a prestained protein marker (Cell Signaling, Beverly, MA) and then transferred to nitrocellulose (Sartorius, Goettingen, Germany). Blots were cut just above the 25-kDa marker; the top half was incubated with a mixture of goat anti-Hsp 60 (Santa Cruz, Heidelberg, Germany), mouse anti-Cox I (Molecular Probes, Leiden, Netherlands), and mouse anti-Porin (Calbiochem), and the bottom half was incubated with a rabbit serum raised against the carboxyl terminus of the x-II ORF (rabbit anti-Tof; 4). After incubation with appropriate horseradish peroxidase-conjugated secondary antibodies (Santa Cruz or Amersham Biosciences), the blots were developed using chemiluminescence detection reagents (Supersignal kit, Pierce) and exposed to Hyperfilm (Amersham Biosciences).

Electron Microscopy—For conventional electron microscopy, p13^{II}-expressing Hltat cells were washed three times in PBS, pH 7.4, and fixed with PBS, 2% glutaraldehyde for 1 h at 4 °C. Samples were postfixed in 1% osmium tetroxide in Veronal acetate buffer, pH 7.4, for 1 h at 25 °C, stained with 0.1% tannic acid in the same buffer for 30 min at 25 °C and with uranyl acetate (5 mg/ml) for 1 h at 25 °C, dehydrated in acetone, and embedded in Epon 812. Thin sections were examined unstained or poststained with uranyl acetate and lead hydroxide. For immunoelectron microscopy, cells were fixed with a mixture of 4% paraformaldehyde and 0.2% glutaraldehyde prepared in 100 mM phosphate buffer for 2 h at 25 °C, washed, placed in 100 mM phosphate buffer containing 12% gelatin (Sigma), and solidified on ice. Gelatin blocks were infused with 2.3 M sucrose overnight at 4 °C, frozen in liquid nitrogen, and cryo-sectioned. Ultrathin cryo-sections were collected with sucrose and methyl cellulose and incubated with rabbit anti-Tof antibody diluted 1:10 in PBS, 1% bovine serum albumin. After several washes in PBS, 0.1% bovine serum albumin, the sections were incubated with 10-nm diameter colloidal gold particles conjugated with goat-anti rabbit IgG (British BioCell International, Cardiff, UK) diluted 1:20 in PBS. Control experiments were performed by omission of the primary antibody from the labeling procedure. After incubation with the antibodies, the cryo-sections were stained with a solution of 2% methyl cellulose and 0.4% uranyl acetate and examined by electron microscopy.

Assays on Isolated Mitochondria—Liver mitochondria isolated from albino Wistar rats weighing about 300 g were prepared by standard centrifugation techniques as described previously (22). Measurements of mitochondrial volume, membrane potential, and Ca^{2+} transport were carried out with a PerkinElmer Life Sciences 650–40 spectrofluorimeter equipped with magnetic stirring and thermostatic control. Mitochondrial volume was measured as the change in 90 ° light scattering at 540 nm (23, 24). Membrane potential and changes in extramitochondrial [Ca^{2+}] were assayed by measuring the change in fluorescence intensity of rhodamine 123 (25) and calcium Green-5N (26), respectively. Both probes were excited at 503 nm (2 nm slit), whereas emission was analyzed at 525 nm for rhodamine 123 and at 535 nm for calcium

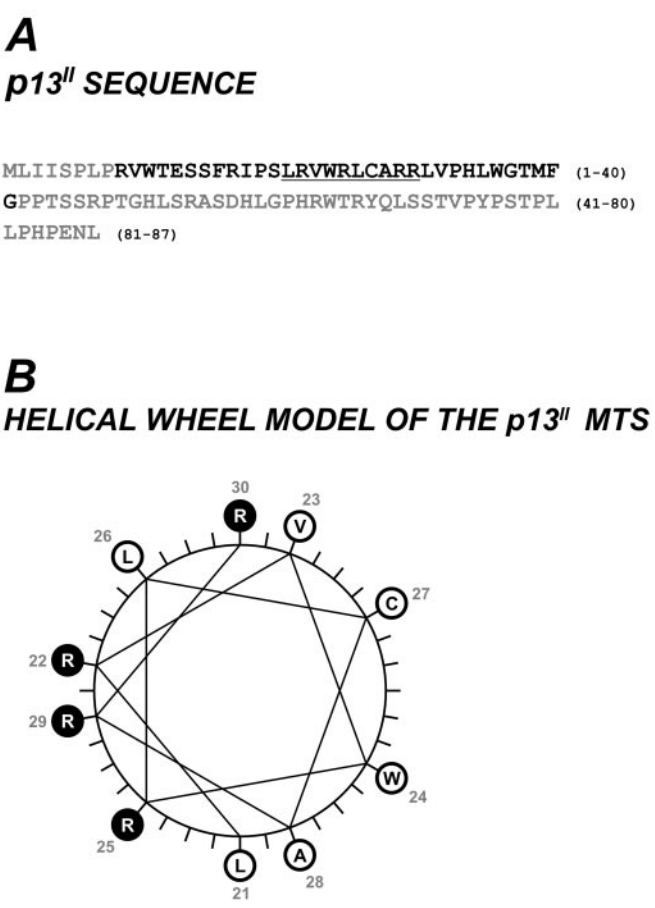

FIG. 1. **The amino acid sequence of p13^{II}.** *Panel A* shows the sequence of p13^{II} coded by molecular clone CS-HTLV-1. The 10-residue MTS shown in a previous study to be sufficient for targeting of green fluorescent protein to mitochondria (residues 21–30; Ref. 13) is *underlined*. The sequence included in the synthetic p13$^{9-41}$ peptide is indicated in *bold*. *Panel B* shows a helical wheel model of the p13^{II} MTS, illustrating partitioning of hydrophobic and positively charged residues on opposite sides of the helix.

Green-5N, with the slit set at 5 nm in both cases. Details of assay conditions are provided in the legends to Figs. 5 and 6.

Indirect Immunofluorescence and Confocal Microscopy—24–36 h after transfection, cells were washed twice with Dulbecco's modified Eagle's medium (DMEM) that had been prewarmed to 37 °C, fixed for 20 min with 3.7% formaldehyde in DMEM, permeabilized for 10 min with 0.1% Nonidet P40/PBS, and then incubated with the antibodies specified in the legend to Fig. 7. Signals were analyzed by confocal microscopy using a LSM510 microscope (Carl Zeiss, Jena, Germany) with argon (488 nm) and helium-neon (543 nm) laser sources and a 63× oil immersion objective; 0.9-μm optical slices were examined.

RESULTS

α-Helical Folding of Synthetic p13^{II} Peptides—Fig. 1*A* shows the 87-amino acid sequence of p13^{II}, with its 10-amino acid MTS underlined. The PHDSec structure prediction program (27) suggests that the amino-terminal portion of the protein contains a short hydrophobic leader (amino acids 1–5) followed by an α-helix (amino acids 21–30) that includes the MTS (13). The latter region includes 4 arginine residues at positions 22, 25, 29, and 30, which are predicted to form a positively charged patch within the putative α-helix, thereby imparting amphipathic properties to this region (Fig. 1*B*; Ref. 13). To directly verify these predictions, we generated synthetic peptides that included the p13^{II} MTS and examined their structure by CD. Results showed that p13$^{9-41}$ (a peptide spanning amino acids 9–41 of wild-type p13^{II}) failed to fold into an ordered structure when placed in an aqueous solution; in particular, the ellipticity minima at 208 and 222 nm that are characteristic of an α helix were not detected under these conditions (Fig. 2*A*). Although the CD spectrum of the peptide changed when recorded in the organic solvent trifluoroethanol, utilized to promote the formation of an α-helical structure, the resulting conformation was predominantly unstructured. In contrast, the spectrum was dominated by the characteristic minima at 208 and 222 nm in the presence of 10 mM SDS, a concentration exceeding the critical micelle concentration, *i.e.* 0.8 mM under the assay conditions employed. The peptide also adopted an α-helical conformation when SDS was replaced with phospholipid vesicles, indicating that the MTS region is able to fold into an α helix only when exposed to a membrane-like environment. Fig. 2*B* shows the influence of the SDS concentration on the CD spectrum of peptide p13$^{9-41}$. Formation of an α helix became evident at an SDS concentration of 0.8 mM, *i.e.* the critical micelle concentration; the ellipticity minima were most pronounced at 1 mM SDS.

As a prelude to subsequent functional studies, we next investigated the folding properties of peptides spanning residues 9–41 in which the 4 arginine residues at positions 22, 25, 29, and 30 were substituted with either 4 glutamines, alanine-leucine-leucine-alanine, or 4 prolines, resulting in peptides p13$^{9-41}$Q, AL, and P, respectively. While the glutamine and alanine-leucine substitution mutants were predicted to retain α helical folding, with just its positively charged face replaced with an uncharged polar cluster (mutant Q) or hydrophobic residues (mutant AL), the proline substitutions were predicted to disrupt the formation of an α helix. As shown in Fig. 2*C*, the spectra of peptides p13$^{9-41}$Q and p13$^{9-41}$AL exhibited minima at 208 and 222 nm in the presence of 10 mM SDS, indicating the formation of an α helix. In contrast, the p13$^{9-41}$P peptide failed to adopt an α-helical conformation.

Submitochondrial Localization of p13^{II}—The finding that peptide p13$^{9-41}$ folded into an α helix when placed in a membrane-like environment prompted us to determine whether p13^{II} is membrane-associated in the context of mitochondria. For this purpose, mitochondria isolated from human cells expressing the full-length p13^{II} protein were extracted with Triton-X-114. This detergent is soluble in aqueous solutions at low temperatures but separates into aqueous and detergent phases above 20°C (20). Mitochondrial proteins partitioned in the aqueous and detergent phases were subjected to SDS-PAGE/immunoblotting and the distribution of p13^{II} was compared with that of the soluble mitochondrial matrix protein Hsp 60 and the membrane proteins Porin and CoxI, which are inserted in the outer and inner mitochondrial membranes, respectively. As shown in Fig. 3*A*, Hsp 60 was detected almost exclusively in the aqueous fraction, while Porin, CoxI, and p13^{II} were found mainly in the detergent fraction, suggesting that p13^{II} is likely to be associated with membranes rather than present in a soluble form in the matrix or intermembrane space.

To test whether p13^{II} was membrane-inserted, we subjected p13^{II}-containing mitochondria to alkaline extraction with sodium carbonate (21) followed by ultracentrifugation through a sucrose step gradient. Fig. 3*B* shows immunoblots of the resulting soluble and membrane-bound fractions carried out to detect p13^{II}, along with Hsp 60, CoxI, and Porin. p13^{II} was detected mainly in the membrane-bound fraction along with the majority of CoxI (not evident in this exposure) and Porin, whereas Hsp 60 was detected mainly in the soluble fraction.

Having obtained evidence that the majority of p13^{II} is membrane-associated, we next determined whether the protein accumulates in the outer or inner membrane on the basis of its sensitivity to extraction by digitonin under isotonic conditions. As shown in Fig. 3*C*, this treatment resulted in partial extrac-

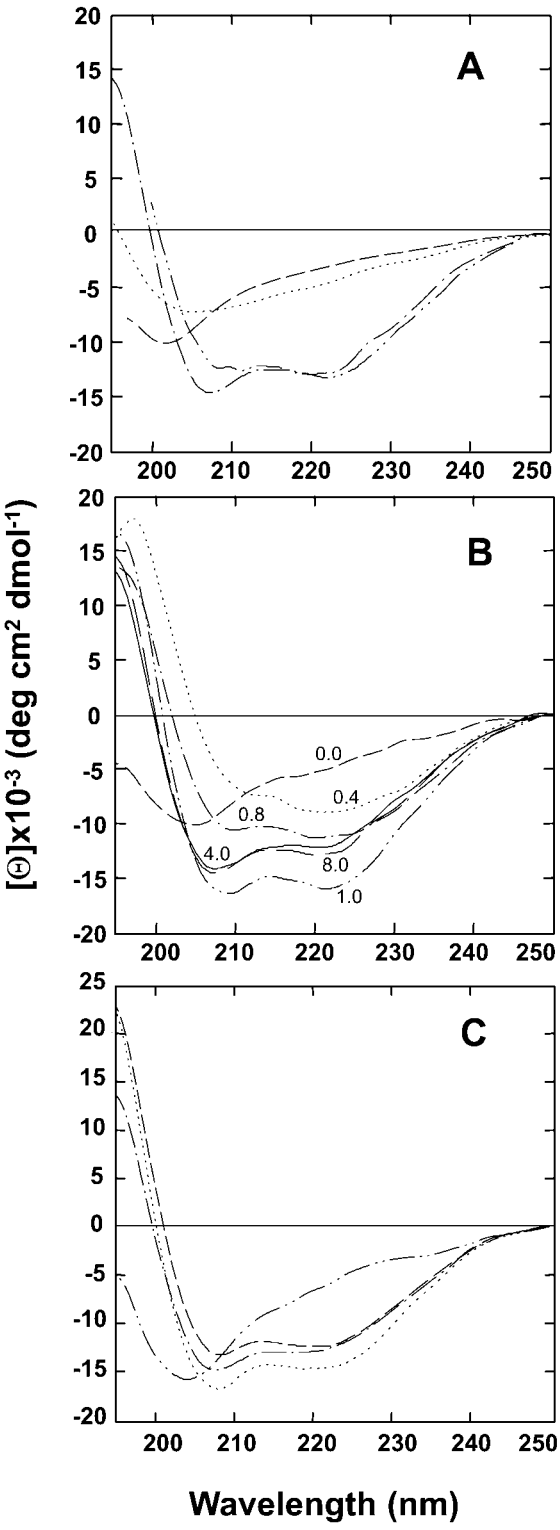

FIG. 2. **Far-UV CD analyses of synthetic peptides spanning the p13^{II} MTS.** *Panel A* shows CD spectra of a peptide spanning amino acids 9–41 of wild-type p13^{II} (p13$^{9-41}$) in different environments: ———,10 mM Tris-HCl, 50 mM NaCl, pH 7.5 (buffer); · · · ·, 40% trifluoroethanol in 5 mM phosphate buffer, pH 7.2; — · —, 10 mM SDS in buffer; — · · —, lipid vesicles in Tris/HCl buffer. *Panel B* shows the influence of increasing SDS concentrations on the CD spectra of peptide p13$^{9-41}$, with the concentration (mM) of SDS indicated near the corresponding spectra. *Panel C* shows CD spectra obtained in the presence of 10 mM SDS for the p13$^{9-41}$ peptide (— · —) and the following peptides containing substitutions of the four arginine residues in the MTS. — — —, p13$^{9-41}$AL; · · · ·, p13$^{9-41}$Q; — · · —, p13$^{9-41}$P. Spectra were measured as described under "Materials and Methods" and normalized as mean residue ellipticity [Θ].

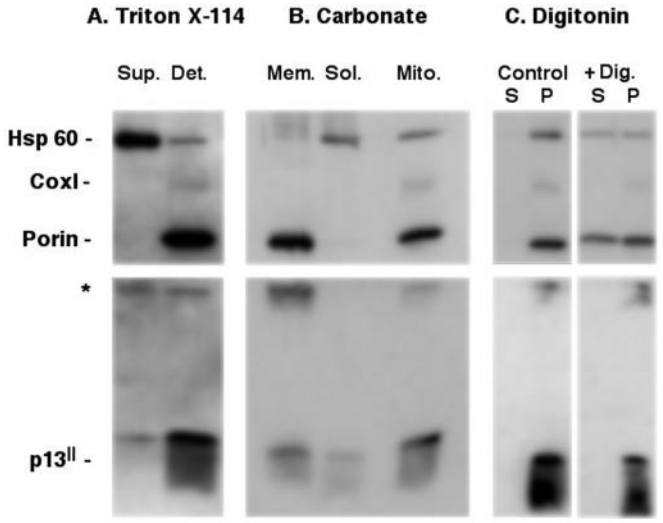

FIG. 3. **Fractionation of mitochondria recovered from p13^{II}-transfected cells.** *Panel A*, mitochondria were extracted with Triton X-114 as described under "Materials and Methods"; the resulting supernatants (*Sup.*) and detergent pellets (*Det.*) were solubilized, separated by SDS-PAGE through a 15% gel, and immunoblotted using antibodies to detect the indicated proteins. *Panel B*, mitochondria were incubated with sodium carbonate and then ultracentrifuged through a step gradient to separate membrane-inserted proteins (*Mem.*) from soluble proteins (*Sol.*) and analyzed by SDS-PAGE/immunoblotting; the *lane* labeled *Mito* contains an aliquot of the mitochondria before treatment. *Panel C*, mitochondria were incubated under isotonic conditions in the absence or presence of digitonin (*Dig.*) and centrifuged, and resulting supernatants (*S*) and pellets (*P*) were analyzed by SDS-PAGE/immunoblotting. The *asterisk* indicates a p13^{II}-related band of about 25 kDa.

tion of the outer membrane protein Porin; in contrast, neither the inner membrane protein CoxI nor p13^{II} was extracted, thus providing evidence that p13^{II} resides in the inner mitochondrial membrane. The immunoblots shown in Fig. 3 also revealed the presence of a p13^{II}-related band of about 25 kDa (denoted by an *asterisk*) of unknown significance (see "Discussion").

To directly visualize the submitochondrial distribution of p13^{II} and to examine its effect on mitochondrial morphology in more detail, electron microscopy was carried out on p13^{II}-transfected human cells (Fig. 4). Immunogold labeling to detect p13^{II} (Fig. 4, *panels A–E*) revealed accumulation of gold particles inside mitochondria, mainly associated with the inner membrane and cristae. This observation supported the results obtained with the biochemical fractionation assays and indicated that the protein accumulates in the inner membrane.

Ultrastructural examination of p13^{II}-transfected cells revealed cells displaying different levels of morphological changes in their mitochondria (Fig. 4, *panels F* and *G*). Although some cells contained apparently unaltered mitochondria, others contained mitochondria showing fragmentation of the cristae and swelling, varying from slight disruption (see mitochondrion labeled *M1*) to substantial or almost complete loss of internal structures (mitochondria labeled *M2* and *M*, respectively). Interestingly, mitochondria exhibiting more prominent alterations often appeared in close proximity to endoplasmic reticulum cisternae (see *arrows* and mitochondria labeled *M* in *panel G*). Although we could not positively identify p13^{II}-expressing cells in this analysis, the percentage of cells showing altered mitochondria was consistent with the percentage of p13^{II}-expressing cells determined by indirect immunofluorescence carried out on an aliquot of the transfected cells (results not shown), thus suggesting an association between p13^{II} expression and the observed ultrastructural changes.

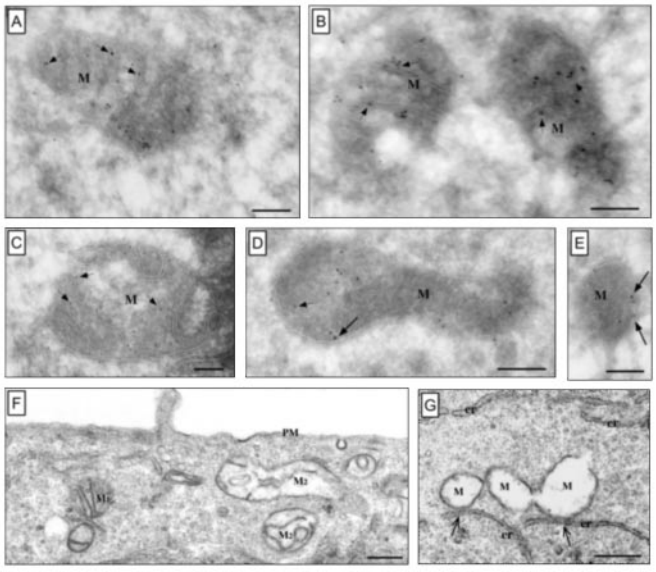

FIG. 4. **Electron microscopy of p13^{II}-expressing cells.** *Panels A–E* show immunoelectron micrographs of mitochondria (*M*) of p13^{II}-transfected Hltat cells prepared as described under "Materials and Methods." The *long arrows* indicate the inner membrane, and the *short arrows* indicate the cristae. *Bar*, 0.2 μm. *Panels F* and *G* show an ultrastructural analysis of p13^{II}-transfected Hltat cells. Slightly disrupted mitochondria are labeled *M1*, and mitochondria showing substantial or almost complete loss of internal structures are labeled *M2* and *M*, respectively. The *arrows* indicate endoplasmic reticulum (*er*) cisternae. *PM*, plasma membrane; *bar*, 0.5 μm.

Cation-dependent Swelling of Isolated Mitochondria Induced by the p13^{II} Peptide—The appearance of the altered mitochondria visualized by indirect immunofluorescence (13) and electron microscopy (Fig. 4, *panels F* and *G*) was suggestive of swelling, a phenomenon that arises from altered permeability of mitochondria to osmotically active species (for review, see Ref. 28). This observation prompted us to assay the effects of the synthetic p13^{II} peptides described above on isolated mitochondria. In the experiments reported in Fig. 5, *panel A*, rat liver mitochondria energized with succinate were incubated in isotonic KCl, and the 90 ° light scattering of the suspension at 540 nm was monitored. The addition of 1 μM wild-type p13$^{9-41}$ peptide (Fig. 5, *panel A*, *trace a*) caused a rapid decrease in light scattering, which is indicative of mitochondrial swelling. After reaching a minimum level of light scattering, mitochondria underwent a partial recovery, and the signal eventually stabilized to an intermediate level. These volume oscillations, which were somewhat variable in extent among different mitochondrial preparations, are typical of the mitochondrial response to cation uptake through a channel, the contraction phase being due to transient activation of the H^+-K^+ exchanger (29) that follows matrix Mg^{2+} dilution (30). Remarkably, swelling was not observed upon the addition of the wild-type p13$^{9-41}$ peptide to mitochondria that had been pretreated with the uncoupler DNP (*panel A*, *trace c*), a treatment that collapses the mitochondrial $\Delta\psi$, indicating that p13$^{9-41}$-mediated swelling required the presence of $\Delta\psi$. p13$^{9-41}$-mediated swelling was substantially reduced when energized mitochondria were incubated in an isotonic sucrose medium rather than in isotonic KCl (*panel A*, *trace e*) but could still be prevented by pretreatment with DNP (results not shown). In contrast to results obtained using the wild-type p13$^{9-41}$ peptide, swelling was not observed when mitochondria were incubated in the presence of p13$^{9-41}$Q or p13$^{9-41}$P, even when the mutated peptides were added at a concentration of 5 μM (*panel A*, *traces b* and *d*, respectively); similar results were obtained using p13$^{9-41}$AL (data not shown). Additional assays showed that a shorter wild-type p13^{II} peptide spanning amino acids 19–33 was able to induce swelling, although to a lesser extent compared with the p13$^{9-41}$ peptide, and that a control peptide similar to p13$^{19-33}$ in length and arginine content (EVRLRGRKRSMLG) was inactive (data not shown).

We next studied the dependence of p13$^{9-41}$-dependent swelling on the K^+ and peptide concentrations as well as on the transport of P_i. Fig. 5, *panel B*, documents that the rate of swelling was a function of the K^+ concentration and revealed an apparent K_m of about 40 mM K^+. Fig. 5, *panel C*, illustrates the dependence of swelling on the concentration of wild-type p13$^{9-41}$ peptide and shows that the half-maximal effect occurred at about 0.4 μM peptide; interestingly, swelling was completely inhibited by blocking P_i transport with *N*-ethylmaleimide, indicating that uptake of substantial amounts of K^+ requires regeneration of $\Delta\psi$ through P_i uptake. It should be noted that in the presence of *N*-ethylmaleimide addition of the wild-type p13$^{9-41}$ peptide was followed by a biphasic response, with a transient swelling phase of short duration followed by a contraction of the same extent (Fig. 5, *panel D*, *trace b*). This is presumably due to the limited K^+ uptake that can occur even in the absence of added P_i and is followed by early activation of the H^+-K^+ exchanger by the high matrix pH reached under these conditions (31).

Additional assays carried out in media of different ionic compositions confirmed that substantial swelling required the presence of P_i and that it occurred when the medium contained small cations like Na^+, tetramethylammonium, and choline but not Tris or larger cations. Taken together, these data demonstrate that p13$^{9-41}$ induces a $\Delta\psi$-driven influx of small cations into mitochondria.

Mitochondrial swelling and altered permeability due to opening of the permeability transition pore (PTP) have recently been demonstrated to play a key role in triggering apoptotic cell death. We therefore asked whether, in analogy to observations made for the viral proteins Vpr of human immunodeficiency virus type 1 and X of hepatitis B virus (for review, see Ref. 32), the PTP might contribute to p13$^{9-41}$-dependent ion transport. To this end, mitochondria were treated with CsA, a known inhibitor of PTP opening, before the addition of p13$^{9-41}$. Results yielded a trace virtually identical to that obtained in the absence of the inhibitor (data not shown), indicating that this swelling process was unaffected by CsA and, thus, arguing against a PTP-mediated mechanism of action for p13$^{9-41}$.

The p13^{II} Peptide Induces a Collapse of $\Delta\psi$—We next asked if the alterations induced by the wild-type p13$^{9-41}$ peptide would result in a collapse of the proton gradient across the inner membrane. To this end we employed the rhodamine 123-quenching assay (25). In this assay, energized mitochondria are added to a cuvette containing rhodamine 123, which is accumulated in the mitochondrial matrix in response to the $\Delta\psi$, resulting in quenching of the red fluorescent signal of the probe (Fig. 6, *panel A*). The addition of p13$^{9-41}$ was followed by a rapid recovery of the rhodamine 123 fluorescence resulting from release of the probe from the mitochondria and indicating depolarization (*panel A*, *trace a*). In contrast, $\Delta\psi$ remained high upon the addition of p13$^{9-41}$Q or p13$^{9-41}$P (*panel A*, *trace b*) and could only be collapsed by the subsequent addition of DNP. Taken together, these results indicate that cation uptake after the increased inner membrane conductance induced by the wild-type p13^{II} peptide leads to mitochondrial depolarization. The results obtained with the mutant peptides indicated that the arginines within the MTS are essential for these effects, thereby substantiating the results of the swelling assays.

The p13^{II} Peptide Permeabilizes Mitochondria to Ca^{2+}—Be-

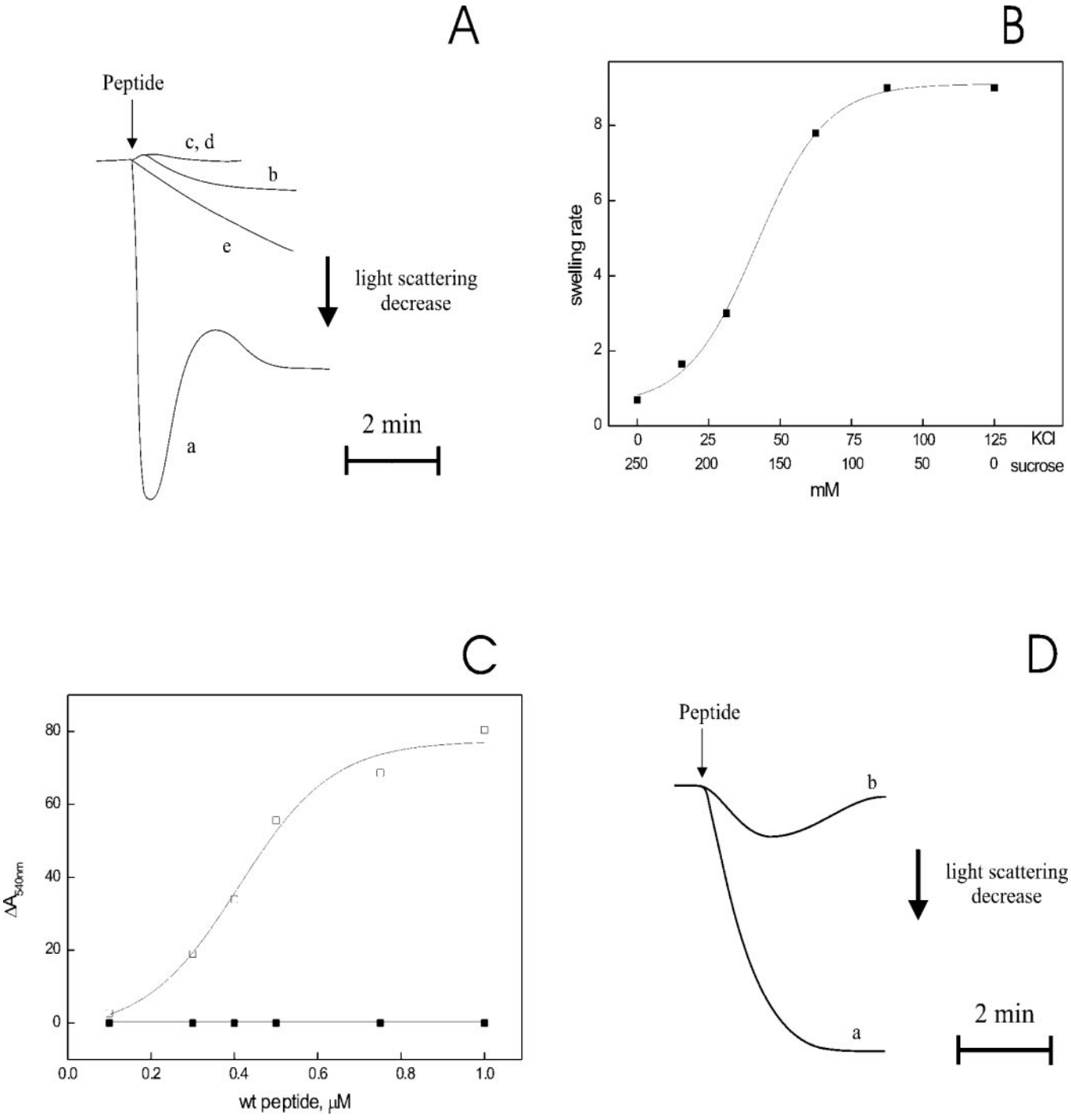

FIG. 5. **Effect of p13^{II} peptides on K^+ permeability and mitochondrial volume.** *Panel A*, swelling assays were performed at 25 °C in a 2-ml final volume containing 125 mM KCl, 10 mM Tris-MOPS, pH 7.4, 1 mM P_i-Tris, 20 μM EGTA-Tris, 5 mM succinate-Tris, and 2 μM rotenone. In *trace e*, KCl was replaced with 250 mM sucrose. One milligram of rat liver mitochondria was added (not shown) followed by the addition (indicated by *vertical arrow*) of 1 μM wild-type p13$^{9-41}$ (*traces a*, *c*, and *e*) or 5 μM p13$^{9-41}$Q (*trace b*) or p13$^{9-41}$P (*trace d*). In *trace c* mitochondria were pretreated with 0.2 mM DNP. *Panel B*, swelling assays were carried out as described for *panel A* with the KCl and sucrose concentrations indicated on the *abscissa*. The rate of swelling induced by 1 μM p13$^{9-41}$ was measured as the change in light scattering at 540 nm/min/mg of total protein. Values of the *ordinate* are in arbitrary units. *Panel C*, end-point swelling values refer to the difference in light scattering at 540 nm measured 5 min after the addition of increasing concentrations of p13$^{9-41}$ in the absence (*open squares*) or presence (*solid squares*) of 25 μM *N*-ethylmaleimide. *Panel D*, the *traces* show the light scattering changes after the addition of 0.5 μM p13$^{9-41}$ in KCl media in the absence (*trace a*) or presence (*trace b*) of *N*-ethylmaleimide.

cause Ca^{2+} is widely recognized to play a key role in intracellular signaling, we next tested whether the p13$^{9-41}$ peptide could affect mitochondrial conductance to Ca^{2+} using an assay based on the fluorescence of the Ca^{2+} indicator calcium green (Fig. 6, *panel B*). Mitochondria were preloaded with a Ca^{2+} pulse in a sucrose-based incubation medium containing CsA (to prevent PTP opening that would normally follow matrix accumulation of Ca^{2+}); ruthenium red was added after completion of Ca^{2+} uptake to block the Ca^{2+} uniporter. As shown in *trace a*, the addition of 1 μM p13$^{9-41}$ caused immediate release of the accumulated Ca^{2+}. This effect was not due to a peptide-dependent collapse of the membrane potential, because Ca^{2+} efflux could not be elicited under these assay conditions by DNP (*trace b*). It is noteworthy that the wild-type peptide remained

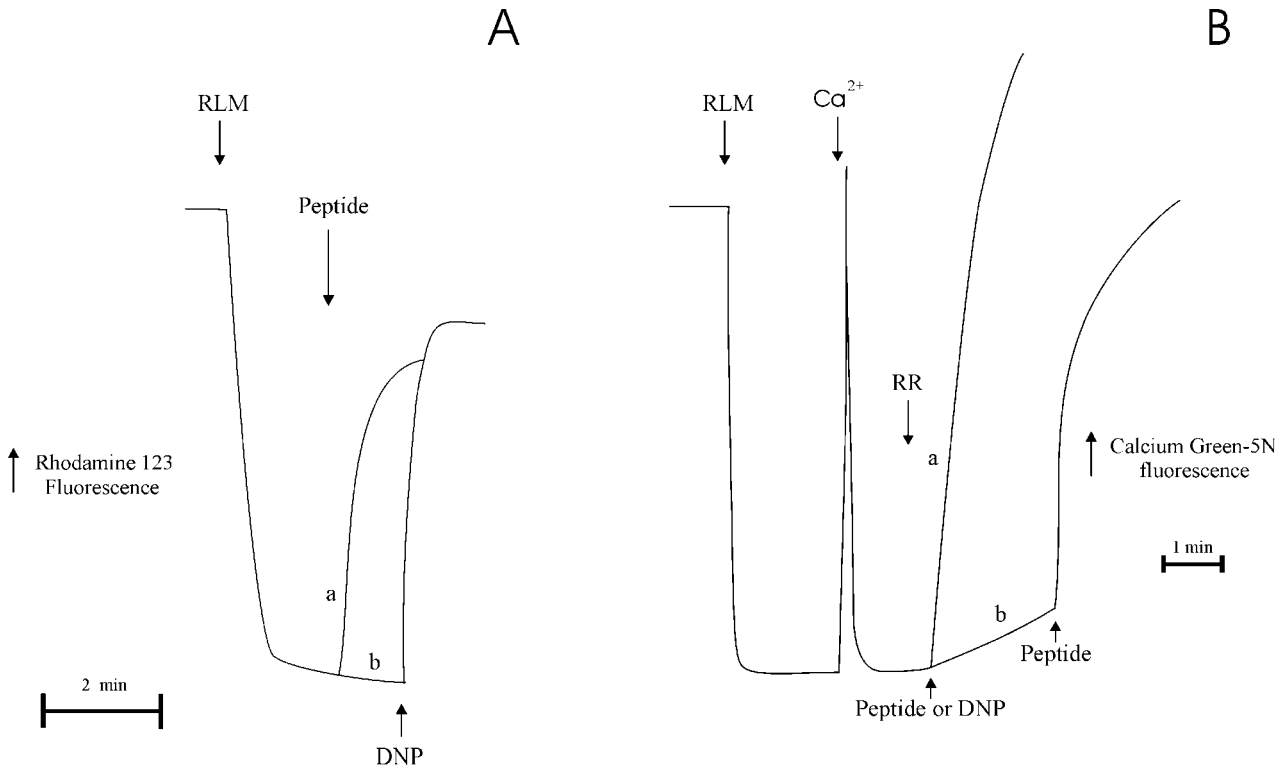

FIG. 6. **Effects of p13^{II} peptides on membrane potential and Ca^{2+} fluxes in isolated mitochondria.** *Panel A*, the experimental conditions were as in Fig. 5, *panel A*, but the medium was supplemented with 0.1 μM rhodamine 123. One milligram of rat liver mitochondria (*RLM*) was added followed by 1 μM wild-type p13$^{9-41}$ peptide (*trace a*); in *trace b*, the mitochondria were treated with 5 μM p13$^{9-41}$Q or p13$^{9-41}$P peptide followed by 200 μM DNP. Values on the *ordinate* refer to changes in rhodamine 123 fluorescence. In *panel B*, assays were performed at 25 °C in a 2-ml final volume containing 250 mM sucrose, 10 mM Tris-MOPS, 1 mM P_i-Tris, 2 μg/ml CsA, 5 mM succinate-Tris, 2 μM rotenone, and 1 μM calcium Green-5N. The following additions (indicated by *arrows*) were made: 1 mg rat liver mitochondria (*RLM*), 10 μM Ca^{2+}, 0.2 μM ruthenium red (*RR*), 1 μM wild-type p13$^{9-41}$ peptide (*trace a*), 0.2 mM DNP (*trace b*) followed by 1 μM wild-type p13$^{9-41}$ peptide (last addition).

effective at discharging Ca^{2+} in mitochondria treated with DNP, suggesting that $\Delta\psi$ is not strictly required for targeting and function of the peptide (*trace b*, last addition). Furthermore, the effect was selective for the wild-type p13$^{9-41}$, because no Ca^{2+} release was observed upon the addition of 5 μM p13$^{9-41}$Q peptide (data not shown).

The Importance of Arginines in the α-Helical MTS for p13^{II} Targeting and Function in Situ—Having obtained evidence that the four arginines in the MTS were involved in triggering cation fluxes in isolated mitochondria, we tested whether these residues were also necessary for p13^{II} to induce changes in mitochondrial morphology *in situ*. To this end, we constructed plasmids coding for full-length p13^{II} containing the glutamine, alanine-leucine, and proline substitutions described above as well as a mutant containing four glutamic acids instead of the four arginines and analyzed their subcellular distribution and effects on mitochondrial morphology in transfected cells subjected to dual staining with antibodies recognizing Hsp 60 and p13^{II} (Fig. 7, *red* and *green* signals, respectively). As demonstrated before, accumulation of wild-type p13^{II} in mitochondria induced alterations in their morphology and distribution that ranged from slight disruption of the network-like pattern to marked swelling and fragmentation into spheroid or ring-shaped structures (Fig. 7, *WT*). Among the mutants tested, only the glutamic acid mutant (E) showed greatly reduced accumulation in mitochondria. The glutamine mutant (Q) induced only a limited degree of mitochondrial fragmentation in a minority of the cells, and the proline mutant (P) showed minor impairment of its mitochondrial-targeting properties with a partial cytosolic localization and failed to change the morphology of mitochondria. The alanine-leucine mutant (AL) also showed a slight impairment in mitochondrial targeting, with some signal appearing in the nuclear envelope and endomembranes; interestingly, instead of fragmenting mitochondria, this mutant appeared to enhance their filiform appearance. Taken together, these results indicate that although the four arginines and the integrity of the α helix itself are not strictly required for mitochondrial targeting, they play a critical role in p13^{II} function, as defined by its ability to induce changes in mitochondrial morphology.

DISCUSSION

Results of the present study indicate a mechanistic basis for our previous observation that p13^{II} causes alterations in mitochondrial morphology suggestive of swelling and fragmentation (13). We have now demonstrated that p13^{II} accumulates in the inner mitochondrial membrane and that p13$^{9-41}$, which includes the MTS, folds into an α helix in the context of a membrane-like environment and has specific effects on the permeability of isolated mitochondria to small cations. This latter effect requires the presence of four arginines within the MTS, a feature that is also essential for the full-length protein to induce changes in mitochondrial morphology in transfected cells, but is not strictly required for mitochondrial targeting. Results of CD analyses demonstrated that efficient α-helical folding of p13$^{9-41}$ requires the presence of detergent or phospholipid micelles to mimic the membrane environment (Fig. 2), thus suggesting that correct folding of full-length p13^{II} might require interaction with or embedding into membranes.

In line with the CD data suggesting membrane-directed folding of p13$^{9-41}$, immunogold analysis (Fig. 4) and extraction of mitochondria-enriched fractions with Triton X-114, sodium carbonate, and digitonin (Fig. 3) indicated that full-length p13^{II} is mainly membrane-associated and accumulates in the inner

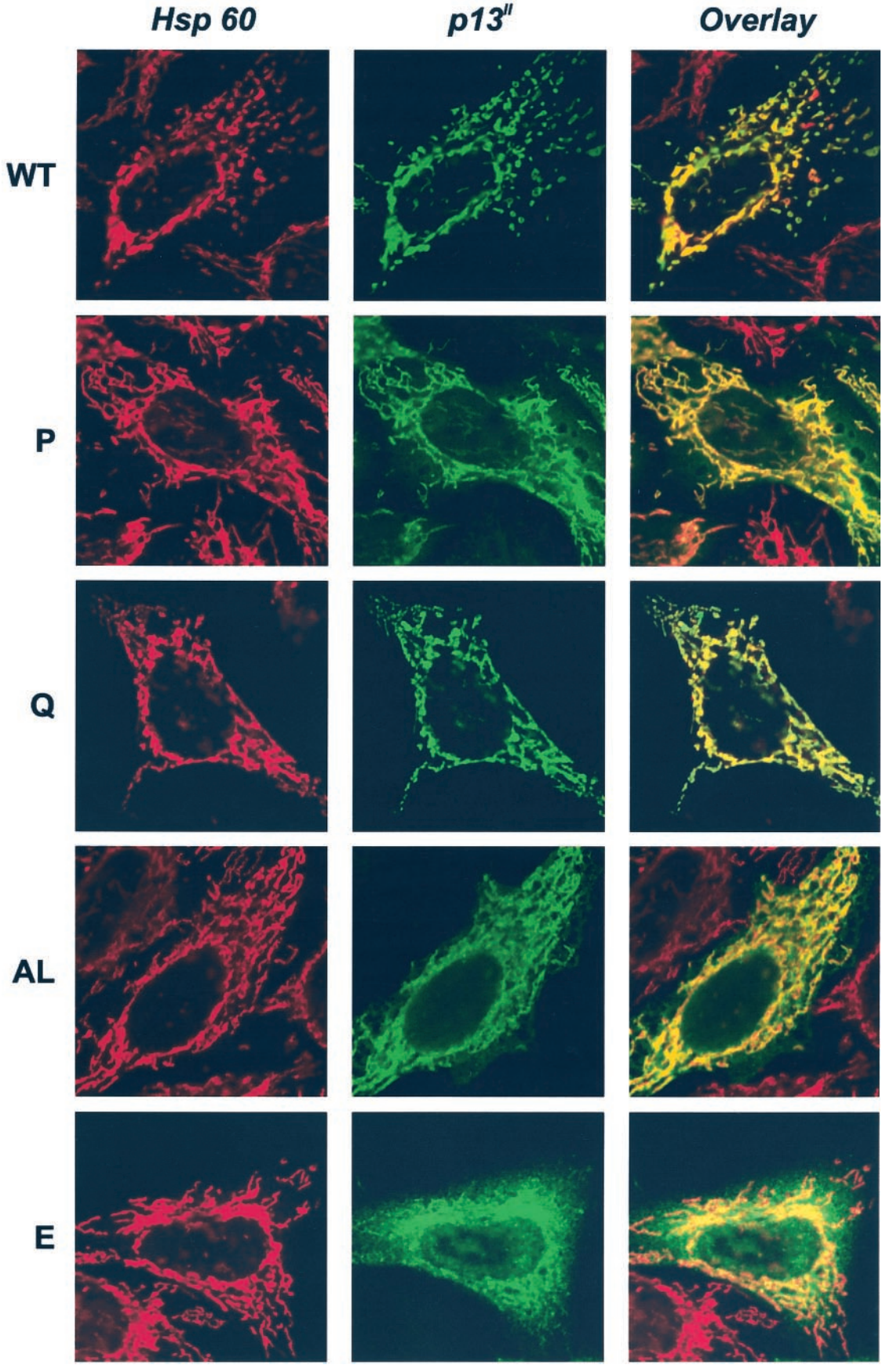

FIG. 7. **Subcellular targeting of wild-type and mutant p13^{II}; effects on mitochondrial morphology.** Shown are the results of indirect immunofluorescence assays to detect wild-type p13^{II} and proline, glutamine, alanine-leucine-leucine-alanine, and glutamic acid substitution mutants (P, Q, AL, and E, respectively) in HeLa cells. p13^{II} (*green signal*) was detected using rabbit anti-Tof followed by Alexa 488-conjugated chicken anti-rabbit antibody (Molecular Probes), and Hsp 60, serving as a marker for mitochondria, was detected using goat anti-Hsp 60 (Santa Cruz) followed by Alexa 546-conjugated donkey anti-goat antibody (Molecular Probes).

mitochondrial membrane. The sodium carbonate extraction method indicated that p13^{II} is present both in membrane-bound and soluble forms (Fig. 3*B*), whereas CoxI and Porin were nearly exclusively found in the membrane fraction. The fraction of p13^{II} that is not membrane-bound may represent the pool of p13^{II} en route to membrane insertion, a feature that might be accentuated under the transient expression conditions used in the present analysis. In alternative, membrane insertion of p13^{II} (and induction of morphological changes) might be restricted to a subpopulation of mitochondria and/or controlled by specific signals such as mitochondrial pH or Ca^{2+} concentration, in analogy with endogenous mitochondrial channels such as the PTP and the Ca^{2+} uniporter. This hypothesis would be in line with the observation that the protein induced varying degrees of mitochondrial alterations in different cells and even among different mitochondria within an individual cell, often in apparent association with proximity to the endoplasmic reticulum (Fig. 4*G*).

The higher molecular weight form of p13^{II} detected in immunoblots was enriched in the membrane-bound fraction obtained after sodium carbonate treatment (Fig. 3*B*) and is consistent with a p13^{II} dimer. Whether this form represents a *bona fide* p13^{II}-p13^{II}dimer, a complex with other proteins, or rather, results from natural post-translational modifications of p13^{II} or chemical modifications arising during mitochondrial isolation is under investigation. In this connection it is worth mentioning that interactions between p13^{II} and cellular proteins have been described in a yeast 2-hybrid screen (33). This analysis identified two binding partners for p13^{II} coded by the K34 molecular clone, C44, a protein that shows substantial similarities to archaeal adenylate kinases, and C254, a protein that probably corresponds to non-muscle filamin. Although the significance of these interactions is unclear, it is noteworthy that eukaryotic adenylate kinase, a probable evolutionary descendent of archaeal adenylate kinases, is a mitochondrial protein involved in energy metabolism. A more recent study demonstrated that p13^{II} also binds to farnesyl pyrophosphate synthetase, an enzyme involved in the mevalonate/squalene pathway, and in the synthesis of farnesyl pyrophosphate, a substrate required for prenylation of Ras (34). This property is shared by G4, a mitochondrially targeted accessory protein expressed by bovine leukemia virus, another complex retrovirus that is classified with HTLV-1 in the Deltaretrovirus genus. Although its biological role remains to be fully understood, G4 is required for efficient propagation of BLV *in vivo* (35) and enhances the oncogenic potential of Ras in the rat embryo fibroblast model of transformation (36). More detailed studies of the interactions between p13^{II} and C44, C254, and farnesyl pyrophosphate synthetase are likely to shed further light on p13^{II}'s function and on viral interference with mitochondrial physiology.

The functional relevance of inner membrane insertion of p13^{II} is supported by our findings on the effects of the synthetic peptides on mitochondria *in vitro*. The portion of p13^{II} spanning residues 9–41 is sufficient to induce rapid, energy-dependent swelling of isolated mitochondria that is sustained by $\Delta\psi$-driven influx of K^+, which requires P_i uptake (Fig. 5). In addition, the p13$^{9-41}$ peptide induces rapid efflux of Ca^{2+} from Ca^{2+}-preloaded mitochondria (Fig. 6*B*). All of these effects critically depend on the presence of the four arginines in the MTS. Whether increased cation conductance reflects an intrinsic ion-conductive property of the peptide or, rather, peptide-dependent opening of native ion channels remains to be determined. We note, however, that cation flux was not affected by ruthenium red, which inhibits both the Ca^{2+} uniporter and the unselective channels for monovalent cations (28), or by CsA, which inhibits the PTP. Although sensitivity of the pore to CsA is not always a safe criterion, we tend to exclude PTP opening as the mechanism underlying swelling because PTP-mediated swelling is not prevented by depolarization with uncouplers, in contrast to p13$^{9-41}$-mediated swelling, which is an active process driven by $\Delta\psi$. Furthermore, the charge and size cut-offs determined in p13$^{9-41}$-mediated swelling experiments underscore a clear distinction from the PTP, which is unselective for charge and has a molecular mass cut-off above about 1,500 Da.

Our efforts to extend the *in vitro* assays to full-length p13^{II} have to date been unsuccessful due to difficulties encountered in producing sufficient quantities of the protein by either chemical synthesis or expression in bacteria. At present, we can, therefore, only extrapolate our observations with p13$^{9-41}$ to full-length p13^{II} based on the overall consistency and the similar sequence requirements of the effects observed *in vitro* and the changes detected *in situ*. In particular, we have shown that expression of full-length p13^{II} in human cells induces mitochondrial changes *in situ* consistent with swelling (Figs. 4 and 7) and mitochondrial depolarization (13). Furthermore, introduction of targeted substitution mutations within the charged portion of the amphipathic α-helical region revealed similar sequence requirements for effects exhibited by the peptide *in vitro* and for morphological changes induced by the protein in cells. *In situ* analyses of amino- and carboxyl-terminal deletion mutants showed that residues amino-terminal to amino acid 18 and carboxyl-terminal to amino acid 56 were dispensable for targeting of p13^{II} to mitochondria and induction of morphological changes, suggesting that p13$^{9-41}$ is likely to span the active portion of the protein (Ref. 13 and data not shown). Interestingly, a shorter p13^{II} peptide that included only the MTS (residues 19–33) was significantly less potent in inducing mitochondrial swelling (data not shown).

Assuming this extrapolation to be valid, the lack of involvement of the PTP in p13$^{9-41}$-driven cation fluxes would underscore an important functional difference between p13^{II} and two other viral proteins recently described to accumulate in mitochondria, namely the hepatitis B virus X protein and human immunodeficiency virus type 1 Vpr (for review, see Ref. 32). Expression of the X protein triggers a redistribution of p53 from the nucleus to perinuclear mitochondrial clusters and induces mitochondrial depolarization, cytochrome *c* release, and apoptosis (37, 38). The X protein physically interacts and colocalizes with HVDAC3, a member of the voltage-dependent anion channel family of proteins, which is one of the candidates for PTP formation or opening (38), and leads to Ca^{2+}-dependent activation of Pyk2, a protein kinase involved in the pathway leading to activation of Src (39). Vpr has been detected in virions, in the nucleus, and in mitochondria, where it triggers PTP-dependent collapse of $\Delta\psi$, release of cytochrome *c*, and apoptosis. These effects require the carboxy-terminal portion of the protein (40) and may critically depend on binding to the intermembrane face of the adenine nucleotide translocase, which forms large conductance channels in phospholipid bilayers (41). At variance from protein X and Vpr, we have no evidence that p13^{II} causes substantial cytochrome *c* release (13), leading us to speculate that the protein may interfere with other mitochondrial functions. Ca^{2+} signaling and Ca^{2+}-dependent regulation of the oxidative phosphorylation machinery (for review, see Ref. 42) are prominent possible targets in light of the effect of p13$^{9-41}$ on mitochondrial permeability to this cation.

The effects of the p13^{II} peptide on isolated mitochondria bear resemblance to those induced by a synthetic peptide corresponding to the signal peptide of CoxIV. A series of studies has demonstrated that peptides corresponding to the CoxIV leader sequence induce swelling and depolarization of isolated brain

and liver mitochondria (43, 44). This process resulted from increased permeability to small cations such as K^+, Na^+, tetraethyl ammonium, or lysine and was dependent on P_i or acetate; these peptides also increased permeability to sucrose and mannitol, but the extent of permeabilization was much lower than that observed with cations. These processes were not blocked when the PTP was inhibited by CsA and were specific for peptides with correctly spaced arginine residues (43, 44). As proposed by Lu and Beavis (44), the leader peptide might play a role in opening a channel through which the CoxIV precursor is imported and/or might be involved in the control of mitochondrial K^+ levels during mitochondrial biogenesis.

There appear to be several analogies between the mitochondrial effects of p13$^{9-41}$ and those of the CoxIV leader peptide. Among these, formation of an amphipathic α-helical structure, cation selectivity, energy dependence of transport, requirement for P_i, and lack of inhibition by CsA suggest that the same channel(s) may be involved. Yet the functional consequences may be different due to the presumably transient nature of the permeability changes induced by the CoxIV leader peptide (44), which is cleaved upon import of the protein. We have no evidence that mitochondrial targeting of p13^{II} involves cleavage. This conclusion is based on the similar electrophoretic mobilities exhibited by p13^{II} expressed in Hltat cells, in *Escherichia coli* and by *in vitro* transcription-translation (13); furthermore, we did not detect differences in the apparent size of p13^{II} in the membrane-bound and unbound mitochondrial fractions shown in Fig. 3*B*. Therefore, the likely possibility that the active region of p13^{II} is retained after targeting suggests that it might exert its function in the context of the mature protein inserted in the inner membrane.

When considered together, the results of the *in vitro* studies performed with the p13^{II} peptides and the targeting and functional properties of full-length wild-type and mutant p13^{II} proteins *in situ* (Fig. 7) indicate that the presence of the four arginines in the MTS are essential for the increase in mitochondrial ion conductance and *in situ* effects on mitochondrial morphology but not for mitochondrial targeting. Our data support a working model in which insertion of p13^{II} in the inner mitochondrial membrane might direct α-helical folding of the MTS in the phospholipid bilayer. This folding in turn might determine the formation of p13^{II} complexes that create a channel-like structure or influence the conductance of an endogenous channel for small cations. These findings, thus, provide mechanistic clues regarding the consequences of the interaction of p13^{II} with mitochondria and provide a groundwork for future studies aimed at determining the impact of these alterations on mitochondrial and cellular physiology within the context of HTLV-1 replication and pathogenesis.

Acknowledgments—We thank Lorenza Zotti for contributing to initial experiments, Tatiana Zorzan for technical assistance, Daniela Saggioro for helpful discussions, Luc Willems for critical reading of the manuscript, and Pierantonio Gallo for artwork.

REFERENCES

1. Johnson, J. M., Harrod, R., and Franchini, G. (2001) *Int. J. Exp. Pathol.* **82,** 135–147
2. Green, P. L., and Chen, I. S. Y. (2001) in *Fields Virology* (Knipe, D. M., Howley, P. M., Griffin, D. E., Lamb, R. A., Martin, M. A., Roizman, B., and Straus, S. E. eds) pp. 1941–1969, 4th Ed., Lippincott-Raven Publishers, Philadelphia
3. Berneman, Z. N., Gartenhaus, R. B., Reitz, J. M. S., Blattner, W. A., Manns, A., Hanchard, B., Ikehara, O., Gallo, R. C., and Klotman, M. E. (1992) *Proc. Natl. Acad. Sci. U. S. A.* **89,** 3005–3009
4. Ciminale, V., Pavlakis, G. N., Derse, D., Cunningham, C. P., and Felber, B. K. (1992) *J. Virol.* **66,** 1737–1745
5. Koralnik, I. J., Gessain, A., Klotman, M. E., Lo Monico, A., Berneman, Z. N., and Franchini, G. (1992) *Proc. Natl. Acad. Sci. U. S. A.* **89,** 8813–8817
6. Derse, D., Mikovits, J., and Ruscetti, F. (1997) *Virology* **237,** 123–128
7. Robek, M. D., Wong, F.-H., and Ratner, L. (1998) *J. Virol.* **72,** 4458–4462
8. Collins, N. D., D'Souza, C., Albrecht, B., Robek, M. D., Ratner, L., Ding, W., Green, P. L., and Lairmore, M. D. (1999) *J. Virol.* **73,** 9642–9649
9. Collins, N. D., Newbound, G. C., Albrecht, B., Beard, J. L., Ratner, L., and Lairmore, M. D. (1998) *Blood* **91,** 4701–4707
10. Bartoe, J., Albrecht, B., Collins, N. D., Robek, M. D., Ratner, L., Green, P. L., and Lairmore, M. D. (2000) *J. Virol.* **74,** 1094–1100
11. Albrecht, B., Collins, N. D., Burniston, M. T., Nisbet, J. W., Ratner, L., Green, P. L., and Lairmore, M. D. (2000) *J. Virol.* **74,** 9828–9834
12. Pique, C., Ureta-Vidal, A., Gessain, A., Chancerel, B., Gout, O., Tamouza, R., Agis, F., and Dokhelar, M.-C. (2000) *J. Exp. Med.* **191,** 567–572
13. Ciminale, V., Zotti, L., D'Agostino, D. M., Ferro, T., Casareto, L., Franchini, G., Bernardi, P., and Chieco-Bianchi, L. (1999) *Oncogene* **18,** 4505–4515
14. Cereseto, A., Berneman, Z., Koralnik, I., Vaughn, J, Franchini, G., and Klotman, M. E. (1997) *Leukemia* (*Baltimore*) **11,** 866–870
15. Fields, G. B., and Noble, R. L. (1990) *Int. J. Pept. Protein Res.* **3,** 161–214
16. Marin, O., Meggio, F., Sarno S., and Pinna L. A. (1997) *Biochemistry* **36,** 7192–7198
17. Derse, D., Mikovits, L., Polianova, M., Felber, B. K., and Ruscetti, F. (1995) *J. Virol.* **69,** 1907–1912
18. Schwartz, S., Felber, B. K., Benko, D. Mfenyo E. M., and Pavlakis, G. N. (1990) *J. Virol.* **64,** 2519–2529
19. Petit, P. X., O'Connor, J. E., Grunwald, D., and Brown, S. C. (1990) *Eur. J. Biochem.* **194,** 389–397
20. Bordier, C. (1981) *J. Biol. Chem.* **256,** 1604–1607
21. Fujiki, Y., Hubbard, A. L., Fowler, S., and Lazarow, P. B. (1982) *J. Cell Biol.* **93,** 97–102
22. Costantini, P., Petronilli, V., Colonna, R., and Bernardi, P. (1995) *Toxicology* **99,** 77–88
23. Hunter, D. R., and Haworth, R. A. (1979) *Arch. Biochem. Biophys.* **195,** 453–459
24. Petronilli, V., Cola, C., Massari, S., Colonna, R., and Bernardi, P. (1993) *J. Biol. Chem.* **268,** 21939–21945
25. Emaus, R. K., Grunwald, R., and Lemasters, J. J. (1986) *Biochim. Biophys. Acta.* **850,** 436–448
26. Fontaine. E., Ichas, F., and Bernardi, P. (1998) *J. Biol. Chem.* **273,** 25734–25740
27. Rost, B., and Sander, C. (1994) *Proteins* **9,** 55–72
28. Bernardi, P. (1999) *Physiol. Rev.* **79,** 1127–1155
29. Bernardi, P., Angrilli, A., Ambrosin, V., and Azzone, G. F. (1989) *J. Biol. Chem.* **264,** 18902–18906
30. Dordick, R. S., Brierley, G. P., and Garlid, K. D. (1980) *J. Biol. Chem.* **255,** 10299–10305
31. Bernardi, P., and Azzone, G. F. (1983) *Biochim. Biophys. Acta* **724,** 212–223
32. Boya, P., Roques, B., and Kroemer, G. (2001) *EMBO J.* **20,** 4325–4331
33. Hou, X., Foley, S., Cueto, M., and Robinson, M. A. (2000) *Virology* **277,** 127–135
34. Lefèbvre, L., Vanderplasschen, A., Ciminale, V., Heremans, H., Dangoisse, O., Jauniaux, J. C., Toussaint, J. F., Zelnik, V., Burny, A., Kettmann, R., and Willems, L. (2002) *J. Virol.* **76,** 1400–1414
35. Willems, L., Kerkhofs, P., Dequiedt, F., Portetelle, D., Mammericks, M., Burny, A., and Kettman, R. (1994) *Proc. Natl. Acad. Sci. U. S. A.* **91,** 11532–11536
36. Kerkhofs, P., Heremans, H., Burny, A., Kettmann, R., and Willems, L. (1998) *J. Virol.* **72,** 2554–2559
37. Takada, S., Shirakata, Y., Kaneniwa, N., and Koike, K. (1999) *Oncogene* **18,** 6965–6973
38. Rahmani, Z., Huh, K.-W., Lasher, R., and Siddiqui, A. (2000) *J. Virol.* **74,** 2840–2846
39. Bouchard, M. J., Wang, L. H., and Schneider, R. J. (2001) *Science* **294,** 2376–2378
40. Jacotot, E., Ravagnan, L., Loeffler, M., Ferri, K. F., Vieira, H. L. A., Zanzami, N., Costantini P., Druillennec, S., Hoebeke, J., Briand, J. P., Irinopoulou, T., Daugas, E., Susin, S. A., Cointe, D., Xie, Z. H., Reed, J. C., Roques, B. P., and Kroemer, G. (2000) *J. Exp. Med.* **191,** 33–45
41. Jacotot, E., Ferri, K. F., El Hamel, C., Brenner, C., Druillennec, S., Hoebeke, J., Rustin, P., Metivier, D., Lenoir, C., Geuskens, M., Vieira, H. L. A., Loeffler, M., Belzacq, A.-S., Briand, J.-P., Zamzami, N., Edelman, L., Xie, Z. H., Reed, J. C., Roques, B. P., and Kroemer, G. (2001) *J. Exp. Med.* **193,** 509–519
42. Rizzuto, R., Bernardi, P., and Pozzan, T. (2000) *J. Physiol.* **529,** 37–47
43. Kushnareva, Y. E., Polster, B. M., Sokolove, P. M., Kinnally, K. W., and Fiskum, G. (2001) *Arch. Biochem. Biophys.* **15,** 251–260
44. Lu, Y., and Beavis, A. D. (1997) *J. Biol. Chem.* **272,** 13555–13561

Mitochondrial Alterations Induced by the p13^{II} Protein of Human T-cell Leukemia Virus Type 1: CRITICAL ROLE OF ARGININE RESIDUES

Donna M. D'Agostino, Laura Ranzato, Giorgio Arrigoni, Ilaria Cavallari, Francesca Belleudi, Maria Rosaria Torrisi, Micol Silic-Benussi, Tiziana Ferro, Valeria Petronilli, Oriano Marin, Luigi Chieco-Bianchi, Paolo Bernardi and Vincenzo Ciminale

J. Biol. Chem. 2002, 277:34424-34433.
doi: 10.1074/jbc.M203023200 originally published online July 1, 2002
